Acta Crystallographica Section A
Foundations of Crystallography
ISSN 0108-7673

Received 31 January 2004
Accepted 13 July 2004

Electronic structure of the nickel(II) complex of the Schiff base of (*S*)-*N*-(2-benzoylphenyl)-1-benzylprolinamide and glycine

Jozef Kožíšek,[a]* Marek Fronc,[a] Pavol Skubák,[a] Alexander Popkov,[b] Martin Breza,[a] Hartmut Fuess[c] and Carsten Paulmann[d]

[a]Department of Physical Chemistry, Faculty of Chemical and Food Technology, Slovak University of Technology, SK-812 37 Bratislava, Slovak Republic, [b]Department of Health Physics and Biophysics, Faculty of Health and Social Studies, University of South Bohemia, CZ-370 05 České Budejovice, Czech Republic, [c]Materials Science, Darmstadt University of Technology, D-642 87 Darmstadt, Germany, and [d]Mineralogisch-Petrographisches Institut, Universität Hamburg, Grindelallee 48, D-20146 Hamburg, Germany. Correspondence e-mail: kozisek@cvt.stuba.sk

The experimental charge density of the Ni^{II} complex of the Schiff base of (*S*)-*N*-(2-benzoylphenyl)-1-benzylprolinamide and glycine was derived from high-resolution single-crystal X-ray diffraction data ($\lambda = 0.5604$ Å) at low temperature (100 K) with synchrotron radiation at the beamline F1 using a CCD area detector. The central Ni atom is pseudo-square-planar coordinated by three N atoms [1.9414 (3), 1.8559 (3) and 1.8533 (3) Å] and by one O atom [1.8620 (4) Å]. The N(1) atom is 0.359 Å above the plane defined by the atoms Ni(1), N(2) and N(3). The *d*-orbital population analysis reveals an oxidation state for the Ni atom of +2 with the configuration d^8 and a hole mainly in the $d_{x^2-y^2}$ orbital, located in the plane of the four ligating atoms. The prochiral reaction centre was examined by topological analysis.

1. Introduction

In the pharmaceutical industry, enantiomerically pure α-methyl amino acids are used as building blocks for peptidomimetic drug design. Owing to environmental constraints, catalytic approaches are favoured as compared to their stoichiometric alternatives. Recent achievements in catalytic asymmetric synthesis of α-methyl amino acids make enantiospecific processes accessible in many cases (Ager, 2002). Less attention is now paid to the development of chiral stoichiometric synthons of α-methyl amino acids for non-industrial purposes. Preparation of ^{11}C-labelled amino acids for positron emission tomography (PET) is an important example (Vaalburg *et al.*, 1976; Plenevaux *et al.*, 1994; Fasth *et al.*, 1995; Långström *et al.*, 1999). Reliable syntheses of compounds labelled with carbon-11 (half-life 20.4 min) are performed on a submicromolar scale in specially designed remote-controlled robotic devices. Limitations brought by very small amounts of a starting compound significantly restrict the applicable procedures. In PET, α-methyl amino acids play a dual role:

(i) as precursors of non-metabolized neurotransmitters (analogues of serotonin, dopamine, tyramine *etc.*) for the study of neurodegenerative diseases;

(ii) as non-metabolized analogues of proteinogenic amino acids for the study of amino acid uptake in normal and cancer cells. Difference in the uptake rates during a PET scan could visualize cancer metastases in a human body.

Clinical applications of such amino acids are very limited due to their poor availability. For the synthesis of the only enantiomerically pure ^{11}C-labelled α-methyl amino acid, α-[^{11}C]methyltryptophan, an industrial procedure was adopted (Crich & Davies, 1989; Bourne *et al.*, 1991; Plenevaux *et al.*, 1994). All attempts to prepare enantiomerically pure α-[^{11}C]methylated tyrosine failed (Gee & Långström, 1991; Rajagopal *et al.*, 1992).

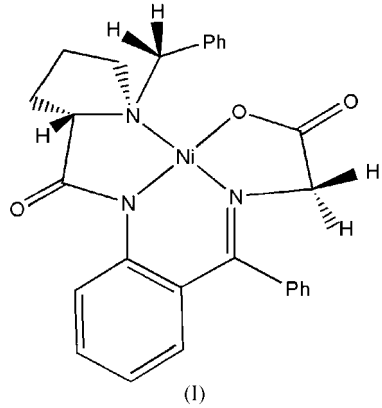

(I)

Our approach to the desired amino acids is based on an improvement of stereodifferentiating the properties of known nickel-based amino acids synthons (Fig. 1) (Belokon, Bakhmutov *et al.*, 1988; Fasth & Långström, 1990; Popkov *et al.*,

2002; Popkov, Nádvorník *et al.*, 2003). Earlier, three ways to meet these goals were suggested.

(i) The first one concerns the conformation of the complexes. As derived from NOE (nuclear Overhauser effect) interactions, the *ortho* protons of the benzyl group are situated closest to the plane of the complex (Jirman & Popkov, 1995). The degree of asymmetric induction of these nickel complexes may be improved by increasing the steric hindrance of the benzyl group by the introduction of methyl substituents in the *ortho* positions.

(ii) The second way concerns the donation of electron density from the π system of the benzyl ring to Ni orbitals. We inferred such a donation of electrons in the complexes. This effect should influence the stereochemical result of alkylation of the complexes under thermodynamically controlled conditions. Two examples supporting our hypothesis were found in the literature: the replacement of the benzyl group in the complex by an electron-rich naphthylmethyl group led to higher asymmetric induction (Belokon, Maleev *et al.*, 1988), whereas the replacement of the benzyl group by various picolyl groups in many cases decreased the induction (De & Thomas, 1997; Blake *et al.*, 2002). We therefore hypothesized that the distance of the benzyl group to the Ni atom will be reduced by the introduction of alkyl substituents in any position on the benzyl group.

(iii) Replacement of the *N*-benzyl group by *N*-(2,4,6-trimethylbenzyl) should disable 'ring-edge' bonding (between the η^2-bonded aromatic ring and the metal atom) due to sterical reasons. Thus only 'ring-centre' bonding where the 2,4,6-trimethylbenzyl group is an 'η^6 ligand' will remain (Popkov *et al.*, 2002).

While the influence of the first factor was proved experimentally and the third one is obvious, existence of the donation of electron density from the π system of the benzyl ring to Ni orbitals is still a hypothesis. This hypothesis was used for explanation of long-range interactions in NMR spectra of ^{13}C- and ^{15}N-labelled complexes (Jirman *et al.*, 1998; Popkov, Langer *et al.*, 2003). In order to estimate this interaction, the electron density from diffraction data has been studied and compared with the theoretical *ab initio* molecular MP2 orbital calculation for an isolated molecule in experimental geometry.

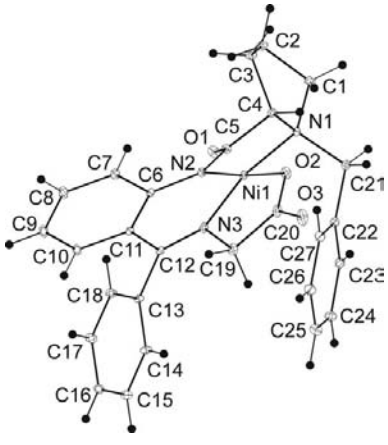

Figure 1
The crystal structure of the title compound with 20% probability thermal displacement ellipsoids (Brandenburg, 1998).

Table 1
Experimental details.

Crystal data	
Empirical formula	$C_{27}H_{25}N_3NiO_3$
Formula weight	498.21
Crystal size (mm)	0.439 × 0.110 × 0.094
Space group	$P2_12_12_1$ (No. 19)
a (Å)	8.9817 (3)
b (Å)	9.6588 (4)
c (Å)	26.2593 (10)
Z	2
Temperature (K)	100.0 (1)
Wavelength (Å)	0.5604
μ (mm^{-1})	0.467
Data collection set	I
Scan type	ω, φ
Max sin θ/λ (Å^{-1})	1.20
Range of indices	
h	−21/21
k	−22/22
l	−59/59
No. of measured diffractions	
after *SAINT*	140195
after *SADABS*	138572
after *XPREP*†	27089
R_{int}	0.0361
$R(\sigma)$	0.0208

† Unique.

2. Experimental

The compound was prepared as described earlier (Nádvorník & Popkov, 2002) and a single crystal was chosen (0.439 × 0.110 × 0.094 mm) and fixed on top of a 0.5 mm glass capillary using UHU-SOFORTFEST glue and a special low-temperature goniometer head. Diffraction data were collected at the synchrotron beamline F1 of the storage ring DORISIII at Hasylab/DESY, Hamburg. Using a wavelength of $\lambda = 0.5604$ Å (Si monochromator) with a Bruker Smart1K CCD detector mounted on the detector arm of a κ diffractometer allowed the collection of 140195 Bragg reflections up to sin $\theta/\lambda = 1.20$ Å^{-1} within 5 d. *SMART*-Kappa 5.A29 software (Bruker, 2001) was used for data collection. During the measurement, the temperature of the crystal was maintained at 100 K. The data reduced to 27089 symmetry-independent reflections. Since a relatively large crystal was used to obtain high-angle data, many low-angle diffractions exceeded the dynamic range of the CCD detector. As a consequence, an Al attenuator was used for a further set of runs for low-angle diffractions in which another 16406 Bragg diffractions were obtained. More details are summarized in Table 1.

3. Data reduction

Orientation matrices for each run were determined by *SMART* software (Bruker, 2001) using about 1000 strongest diffractions equally distributed over the run. Final lattice cell parameters were obtained by weighted least-squares fit of all

Table 2
Summary of least-squares refinements.

Refinement	(I)	(II)	(III)	(IV)
$\sin\theta/\lambda$ (Å^{-1})	0–1.2	0.75–1.2	0–1.2	0–1.2
N_{obs}	26433	18208	26433	26433
N_v	383	382	65	981
$R(F)$	0.0233	0.0226	0.0228	0.0151
$R(F)$†	0.0244	0.0254	0.0239	0.0162
$wR(F)$†	0.0332	0.0238	0.0284	0.0174
$R(F^2)$	0.0399	0.0364	0.0393	0.0217
$R(F^2)$†	0.0399	0.0452	0.0394	0.0218
$wR(F^2)$†	0.0666	0.0469	0.0542	0.0323
S	2.75	1.54	2.67	1.55

† All reflections.

sets of lattice cell parameters for each run. The decrease of the primary-beam intensity was corrected by the local software *SAPRO* (Paulmann, 2001) with simultaneously recorded external monitor data. The intensities were afterwards integrated using the *SAINT* software package (Bruker, 2001). During the integration, each orientation matrix was optimized after every 50 frames. Integrated intensities were further scaled, corrected for the absorption and for some other effects by *SADABS* (Sheldrick, 2002). In the first set, *SADABS* produced 138572 corrected diffractions which were merged by *XPREP* (Bruker, 1997) to 27089 unique diffractions [R_{int} = 0.0361, $R(\sigma)$ = 0.0208]. After truncating at 2.0 Å resolution, the second set (Al attenuator) gave 3955 corrected and finally 297 unique diffractions [R_{int} = 0.0644, $R(\sigma)$ = 0.0334] (see Table 1).[1]

4. Least-squares refinements

Starting parameters were taken from a previous paper (Popkov, Langer *et al.*, 2003) and all refinements were carried out on F^2 using the *XD* (Koritsanszky *et al.*, 1997) suite of programs. The strategy for refinements was as described earlier (Kožíšek *et al.*, 2002). Four different refinements were carried out using statistical weights throughout and the results are summarized in Table 2. Refinement (I) is a traditional independent-atom refinement. Refinement (II) is a high-angle refinement ($0.7 \leq \sin\theta/\lambda \leq 1.20$ Å^{-1}) with the H atoms fixed at the typical distances obtained from neutron diffraction experiments (Allen *et al.*, 1992) and isotropic thermal parameters fixed at the values obtained in refinement (I). Refinement (III) is a κ refinement with the aim of assigning atomic charges (Coppens, 1997). The H-atom positional and thermal parameters were fixed as in refinement (II). A complete atom-centred multipole refinement was carried out in (IV), where the nonspherical atomic electron density (Coppens, 1997) is given by

[1] Supplementary data for this paper are available from the IUCr electronic archives (Reference XC5005). Services for accessing these data are described at the back of the journal.

Table 3
Population of the *d* orbitals.

Orbital	$d_{x^2-y^2}$	d_{z^2}	d_{yz}	d_{xz}	d_{xy}
[e$^-$]	0.36 (2)	1.98 (2)	2.04 (2)	1.82 (2)	1.69 (2)

$$\rho_{at}(r) = P_c\rho_{core}(r) + P_v\kappa^3\rho_{valence}(\kappa r) + \sum_{l=1}^{l_{max}} \kappa'^3 R_l(\kappa' r) \sum_{m=0}^{l} P_{lm\pm} d_{lm\pm}(\theta, \varphi).$$

The H atoms were treated with one bond-directed dipole (l = 1), other atoms were refined up to octupoles, for the Ni atom the hexadecapole level (l_{max} = 4) was used. The local coordinate systems to define multipoles were defined as follows. For non-H atoms: x axis is direction to the closest atom, y axis is perpendicular to the x axis and oriented towards the second closest atom; for H atoms: z axis is direction to the bonding C atom and x axis is perpendicular to the z axis. The same types of H atoms [sp^3 hybridization: H(1), H(2), H(3), H(21); sp^2 hybridization: H(7), H(14) and H(23)] were constrained to have identical multipole expansions.

5. Results and discussion

The central Ni atom is pseudo-square-planar coordinated by three N atoms [N(1), N(2) and N(3), 1.9414 (3), 1.8559 (3) and 1.8533 (3) Å, respectively] and by one O atom [1.8620 (4) Å]. The N(1) atom is 0.359 Å above the plane defined by the atoms Ni(1), N(2) and N(3). As may be seen in Table 2, the multipole refinement achieved a significant improvement of the agreement between the experimental and calculated structure factors. Residual density maps are calculated by a Fourier synthesis where the coefficients are differences between the observed and calculated structure factors corresponding to the converged multipole model. The maximum

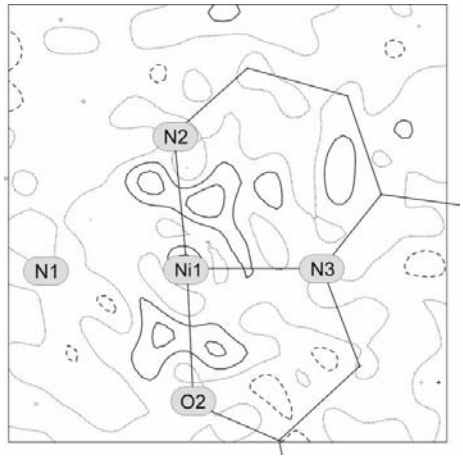

Figure 2
Residual density map in the plane of atoms Ni(1), N(3) and N(2). Positive, negative and zero contours are represented by solid, dashed and dotted curves. Contour spacing 0.05 e Å^{-3}. The maximum positive density in this plane is 0.147 e Å^{-3}, the minimum negative density is −0.074 e Å^{-3}.

Table 4
Electron-density properties at bond critical points.

Bond		Experimental				Theoretical				
Atom *A*	Atom *B*	d_{AB} (Å)	ρ_b (e Å^{-3})	$\nabla^2\rho_b$ (e Å^{-5})	ε	d_A (Å)	d_B (Å)	ρ_b (e Å^{-3})	$\nabla^2\rho_b$ (e Å^{-5})	ε
Ni	O2	1.8620 (4)	0.581 (5)	15.89 (1)	0.03	0.9139	0.9504	0.682	18.700	0.424
Ni	N1	1.9413 (3)	0.522 (5)	11.96 (1)	0.24	0.9344	1.0090	0.668	14.072	0.410
Ni	N2	1.8559 (3)	0.644 (6)	16.60 (1)	0.07	0.8828	0.9736	0.796	17.024	0.222
Ni	N3	1.8533 (3)	0.711 (6)	15.76 (1)	0.07	0.9004	0.9536	0.803	17.284	0.215
O1	C5	1.2288 (5)	2.85 (4)	−38.5 (2)	0.24	0.7771	0.4518	2.605	−13.468	0.032
O2	C20	1.2935 (6)	2.36 (4)	−27.6 (2)	0.16	0.8307	0.4630	2.207	−14.392	0.090
O3	C20	1.2249 (5)	2.76 (4)	−32.5 (2)	0.22	0.7707	0.4543	2.652	−13.728	0.010
N1	C1	1.4925 (5)	1.62 (3)	−7.14 (7)	0.11	0.8380	0.6550	1.552	−9.224	0.049
N1	C4	1.4934 (4)	1.58 (2)	−6.75 (6)	0.08	0.8199	0.6743	1.579	−9.908	0.025
N1	C21	1.5000 (5)	1.56 (2)	−9.32 (7)	0.14	0.8388	0.6613	1.525	−9.148	0.050
N2	C5	1.3750 (4)	2.15 (3)	−21.8 (1)	0.23	0.7856	0.5913	2.031	−17.128	0.032
N2	C6	1.3898 (4)	2.04 (3)	−15.10 (9)	0.13	0.7775	0.6130	1.950	−16.408	0.028
N3	C12	1.2982 (4)	2.56 (3)	−34.6 (2)	0.33	0.7972	0.5016	2.355	−18.180	0.024
N3	C19	1.4689 (4)	1.65 (3)	−9.18 (8)	0.11	0.8360	0.6332	1.579	−9.660	0.048
C1	C2	1.5120 (6)	1.64 (2)	−10.42 (6)	0.12	0.7918	0.7210	1.647	−13.352	0.037
C2	C3	1.5120 (6)	1.61 (2)	−10.22 (5)	0.07	0.7819	0.7509	1.566	−11.732	0.018
C3	C4	1.5553 (5)	1.54 (2)	−8.62 (4)	0.11	0.7651	0.7907	1.518	−10.836	0.032
C4	C5	1.5089 (5)	1.80 (2)	−14.52 (5)	0.22	0.7464	0.7634	1.701	−14.208	0.059
C6	C7	1.4153 (4)	1.99 (2)	−15.18 (6)	0.28	0.7201	0.7030	1.957	−19.048	0.106
C6	C11	1.4212 (4)	2.01 (2)	−17.22 (6)	0.30	0.7183	0.7030	1.930	−18.440	0.155
C7	C8	1.3806 (6)	2.14 (3)	−20.58 (7)	0.30	0.6902	0.6917	2.099	−22.064	0.125
C8	C9	1.3969 (6)	2.13 (3)	−21.22 (7)	0.27	0.7023	0.6950	2.045	−21.148	0.095
C9	C10	1.3817 (5)	2.12 (3)	−20.00 (7)	0.37	0.7025	0.6795	2.112	−22.324	0.134
C10	C11	1.4156 (5)	2.01 (3)	−17.28 (6)	0.29	0.6791	0.7364	1.964	−19.288	0.122
C11	C12	1.4606 (4)	1.85 (2)	−14.26 (5)	0.26	0.7040	0.7567	1.795	−16.116	0.079
C12	C13	1.4964 (4)	1.77 (2)	−12.95 (5)	0.03	0.7584	0.7383	1.694	−14.536	0.013
C13	C14	1.3987 (5)	2.17 (3)	−20.27 (7)	0.26	0.7290	0.6697	1.998	−19.808	0.136
C13	C18	1.3961 (5)	2.17 (2)	−19.54 (7)	0.25	0.6783	0.7179	2.031	−20.560	0.141
C14	C15	1.3949 (6)	2.17 (3)	−21.74 (7)	0.18	0.6779	0.7173	2.031	−20.716	0.113
C15	C16	1.39 44 (7)	2.17 (3)	−21.00 (7)	0.25	0.6725	0.7221	2.045	−21.168	0.106
C16	C17	1.39 39 (7)	2.21 (3)	−19.27 (7)	0.23	0.7130	0.6810	2.058	−21.392	0.109
C17	C18	1.39 54 (5)	2.11 (3)	−18.01 (7)	0.20	0.6828	0.7127	2.018	−20.492	0.112
C19	C20	1.5202 (6)	1.78 (3)	−12.08 (5)	0.15	0.7394	0.7818	1.680	−13.756	0.064
C21	C22	1.5067 (6)	1.75 (2)	−13.24 (5)	0.01	0.7609	0.7358	1.653	−13.756	0.032
C22	C23	1.3973 (7)	2.14 (3)	−20.07 (7)	0.31	0.6788	0.7222	2.018	−20.232	0.128
C22	C27	1.4007 (6)	2.19 (3)	−21.68 (9)	0.19	0.7537	0.6445	2.024	−20.504	0.141
C23	C24	1.3914 (8)	2.19 (3)	−21.5 (1)	0.39	0.7575	0.6357	2.038	−20.908	0.111
C24	C25	1.395 (1)	2.14 (4)	−17.9 (1)	0.38	0.7695	0.6427	2.085	−21.940	0.110
C25	C26	1.404 (2)	2.14 (4)	−19.6 (1)	0.15	0.7595	0.6391	2.072	−21.716	0.108
C26	C27	1.3933 (9)	2.11 (4)	−19.26 (8)	0.17	0.6986	0.6933	2.045	−21.100	0.111

and minimum of the residual density are +0.147 e Å^{-3} at a distance of 1.27 Å from Ni(1) and 0.78 Å from N(2), and −0.074 e Å^{-3} at a distance of 0.58 Å from Ni(1) and 1.33 Å from O(2), respectively; the root-mean-square residual density is 0.032 e Å^{-3} (Fig. 2).

In Figs. 3–7, we present multipole-model static deformation density maps. The equatorial plane (Fig. 3) is defined by the atoms Ni(1), N(3) and N(2). As the atom N(1) is 0.359 Å above this plane, the electron density is not so intensive as for N(2) and N(3). A similar situation is found for O(2) (0.09 Å below). The occupancies of the *d* orbitals calculated from multipole population parameters are given in Table 3. These values are sensitive to a reliable absorption correction. The maximum values should not exceed 2 electrons per orbital; this is a good check of a reliable absorption correction. The *d*-orbital populations in Table 3 are in good agreement with the features observed in Fig. 3 and topological analysis in Table 4: the non-bonding orbitals d_{z^2} and d_{yz} are fully populated. The electron configuration of the Ni atom is nearly d^8; the missing two electrons in the 3*d* shell have been taken to *ca* 80% from the $d_{x^2-y^2}$ orbital. Integration of electron density in the atomic basin by *TOPXD* gives charges for Ni(1) and the following donor atoms: +1.83 for Ni(1), −0.55 for N(1), −0.86 for N(2), −0.88 for N(3) and −0.96 for O(2).

The coordination bond formed by the lone electron pairs of atoms N(1), N(2), N(3) and O(2) point to the space with electron-density depletion (orbital $d_{x^2-y^2}$). Bond strengths correlate with the bonding distances and the values of electron

density ρ_b at bond critical points (BCP) as well. The lowest value of 0.522 (5) e Å^{-3} for N(1) agrees also with the different type of hybridization (sp^3). The ellipticities for all donor atoms indicate mainly σ-bond character, except the Ni(1)—N(1) bond (ε = 0.24). The interatomic distance of 1.9413 (3) Å is significantly longer than Ni(1)—N(2) and Ni(1)—N(3) bonds, so the only explanation is the mechanical strain that deforms the cylindrical symmetry of the σ bond (Bader, 1990). This mechanical strain might be seen also in the adjacent N(1)—C(21) bond with the interatomic distance of 1.5000 (5) Å, which is evidently single (Allen *et al.*, 1992), but its ellipticity is 0.14. The higher value for the N(1)—C(21)—C(22) angle of 113.95 (3)° as compared to the tetrahedral value of 109°28′ and the other angles around the sp^3 C(21) atom (107.7–108.8°) indicates that the benzyl group is pushed away from the Ni^{II} central atom and the ellipticity is a compromise between the sp^3 hybridization of N(1) and this repulsion.

For Ni(1)—O(2), the value of electron density ρ_b (Table 4) is smaller than for the N(2) and N(3) cases (probably due to the higher electronegativity of oxygen). Positive Laplacians $\nabla^2\rho_b$ [11.96 (1)–16.60 (1) e Å^{-5}] indicate strong coordination bonds (Kožíšek *et al.*, 2002; Slouf *et al.*, 2002).

An apparent correlation may be seen when comparing the value of the electron density ρ_b at BCP with the ellipticity. Higher ellipticity values in the case of N(2)—C(5) and C(4)—C(5) bonds are due to the vicinity of the C(5)—O(1) double bond. The highest value for ellipticity at BCP (0.33) was found for the N(3)—C(12) bond, which is evidently double.

In order to examine expected interaction between the benzyl group and the Ni(1) atom [interatomic distances Ni(1)—C(21), Ni(1)—C(22), Ni(1)—C(23) and Ni(1)—C(27) of 2.7836 (4), 2.9397 (4), 3.2817 (5) and 3.6825 (5) Å, respectively], the static deformation density map in the plane of the benzyl group and in the parallel planes (0.3 Å above and below) were calculated (Figs. 4–6). Fig. 4 shows the static electron density in the plane defined by C(22), C(23) and C(27) atoms. The electron density in the plane shifted towards the Ni(1) atom is significantly higher (Fig. 5) than in the

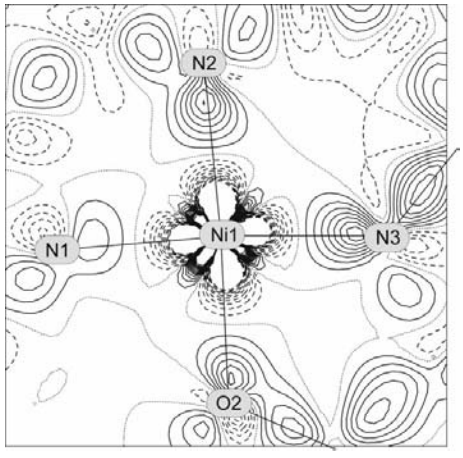

Figure 3
Static electron deformation densities in the plane defined by the atoms Ni(1), N(3) and N(2). Contour spacing 0.1 e Å^{-3}.

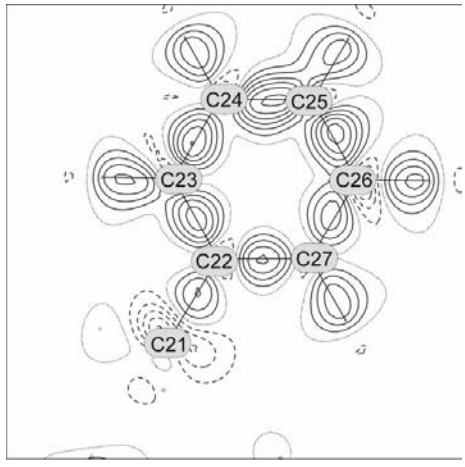

Figure 5
Static electron deformation densities +0.3 Å from the plane defined by the atoms C(22), C(27) and C(23). Contours as in Fig. 3.

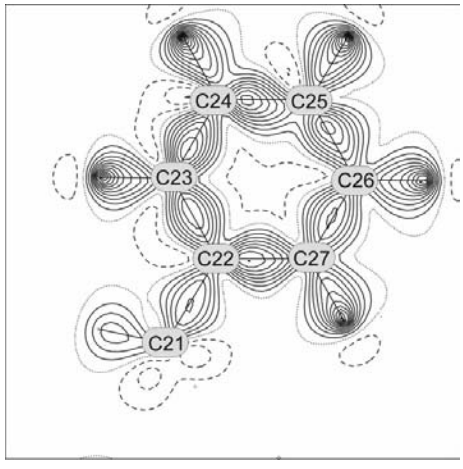

Figure 4
Static electron deformation densities in the plane defined by the atoms C(22), C(27) and C(23). Contours as in Fig. 3.

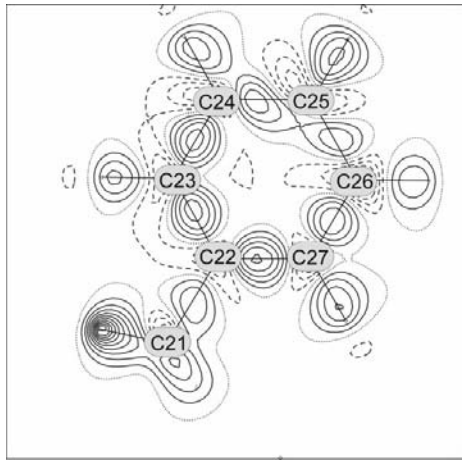

Figure 6
Static electron deformation densities −0.3 Å from the plane defined by the atoms C(22), C(27) and C(23). Contours as in Fig. 3.

opposite direction (Fig. 6) in spite of our expectation (residual Fourier synthesis gave maximum and minimum +0.097 and −0.098 e Å^{-3}, respectively; the root-mean-square residual density is 0.028 e Å^{-3}). To conceive the shape of the area close to the Ni(1) atom in the direction towards the benzyl group, the additional static deformation density map in the plane defined by the atoms Ni(1), C(22) and C(23) was drawn (Fig. 7). The electron density around Ni(1) is mostly in the area of the d_{z^2} orbital (Table 3). The original symmetry of this orbital seems to be lowered by benzyl π-electron repulsion. It might be concluded that no coordination bond between the Ni(1) atom and the benzyl group has been found, but some kind of interaction is evident. Here the question arises whether the electron density pushing into a benzyl group from methyl substituents [similar to the case of the *N*-(2,4,6-trimethylbenzyl) group mentioned above] really supports the desired asymmetric synthesis.

In order to see differences on the prochiral reaction centre, chemical constraints were not applied to atoms H(19*A*) and H(19*B*). Multipole refinement converged with significantly different values for monopoles [for atom H(19*A*) of 1.00 and for H(19*B*) of 0.77]. The residual map in the corresponding plane does not exceed a minimum of −0.11 and a maximum of +0.07 e Å^{-3}, respectively. A shift of the maximum of bonding electron density towards the H atoms (Fig. 8) is in the present study a general feature and might be connected with the systematic error introduced by the scaling and/or weighting procedures of the data with the Al attenuator.

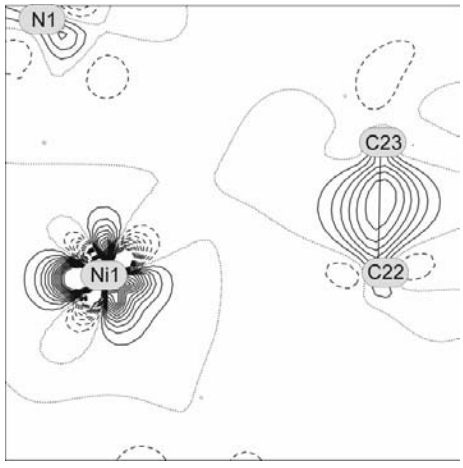

Figure 7
Static electron deformation densities in the plane defined by the atoms Ni(1), C(22) and C(23). Contours as in Fig. 3.

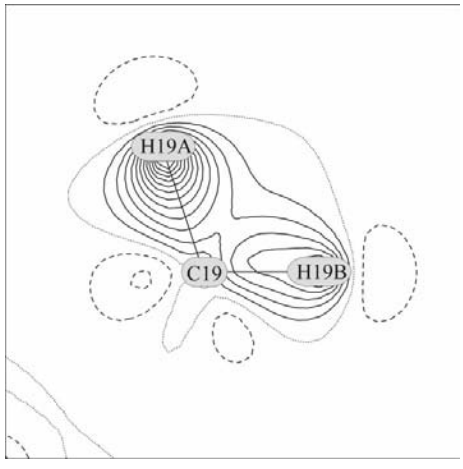

Figure 8
Static electron deformation densities in the plane defined by the atoms C(19), H(19*B*) and H(19*A*). Contours as in Fig. 3.

Ab initio MP2 calculation for the isolated title molecule within experimental geometry has been performed using standard *PC GAMESS* program package (Schmidt *et al.*, 1993; Granovsky, 2003) with TZV basis set for Ni (Rappe *et al.,* 1981) and DZV basis sets for the remaining atoms (Dunning & Hay, 1977). The electronic structure was evaluated in terms of topological analysis of electron density (Bader, 1990) using the *AIM2000* program (Biegler-König *et al.*, 2001; http://www.aim2000.de) such as electron density, Laplacian density and bond ellipticity at the BCP. Comparison of experimental and calculated electron densities (Table 4) exhibits, in general, similar trends. Very good agreement was found for the unsaturated rings as well as for a saturated N(1)—C(1)—C(2)—C(3)—C(4) one. Larger differences may be observed in the Ni(1) coordination polyhedron [especially the Ni(1)—O(2) ellipticity], but the trends in BCP electron density are preserved. Significantly larger differences are in the delocalized subsystems O(2)—C(20)—O(3) and O(1)—C(5)—N(2) as well as in the N(3)—C(12) bond. The greatest portion of these discrepancies might be ascribed to enviromental influences, which are not considered in our quantum-chemical calculations. No bonding paths between the Ni(1) atom and the benzyl group have been found (in agreement with the repulsion interaction indicated by experimental data).

This work was supported by the IHP-Contract HPRI-CT-1999-00040/2001-00140 of the European Commission. The authors thank also the Grant Agency of Slovak Republic, Grants No. 1/9255/02 and 1/0052/03. Part of this work was financed by Ministry of Education, Youth and Sports of the Czech Republic (COST-OCD20.005).

References

Ager, D. J. (2002). *Curr. Opinion Drug Discovery Develop.* **5**, 892–905.

Allen, F. H., Kennard, O., Watson, D. G., Brammer, L., Orpen, A. G. & Taylor, R. (1992). *International Tables for Crystallography*, Vol. C, edited by A. J. C. Wilson, pp. 685–706. Dordrecht/Boston/London: Kluwer Academic Publishers.

Bader, R. F. W. (1990). *Atoms in Molecules. A Quantum Theory*. *International Series of Monographs on Chemistry*, edited by J. Halpen & M. L. H. Green. Oxford: Clarendon Press.

Belokon, Y. N., Bakhmutov, V. I., Chernoglazova, N. I., Kochetkov, K. A., Vitt, S. V., Garbalinskaya, N. S. & Belikov, V. M. (1988). *J. Chem. Soc. Perkin Trans. 1*, pp. 305–312.

Belokon, Y. N., Maleev, V. I., Saporovskaya, M. B., Bakhmutov, V. I., Timofeeva, T. V., Batsanov, A. S., Struchkov, Y. T., Belikov, V. M. (1988). *Koordinat. Khim.* **14**, 1565–1575. (In Russian.)

Biegler-König, F., Schönbohm, J. & Bayles, D. (2001). *J. Comput. Chem.* **22**, 545–559.

Blake, A. J., De, B. B., Li, W. S. & Thomas, N. R. (2002). *Acta Cryst.* C**58**, m570–m574.
Bourne, G. T., Crich, D., Davies, J. W. & Horwell, D. C. (1991). *J. Chem Soc. Perkin Trans. 1*, pp. 1693–1699.
Brandenburg, K. (1998). *DIAMOND. Visual Information System for Crystal Structures*. Bonn, Germany.
Bruker (1997). *XPREP* (Version 5.1/NT). Bruker AXS Inc., Madison, WI, USA.
Bruker (2001). *SMART* (Version 5.A29), *SAINT* (Version 6.26A). Bruker AXS Inc., Madison, Wisconsin, USA.
Coppens, P. (1997). *X-ray Charge Densities and Chemical Bonding.* Oxford University Press.
Crich, D. & Davies, J. W. (1989). *J. Chem. Soc. Chem. Commun.* pp. 1418–1419.
De, B. B. & Thomas, N. R. (1997). *Tetrahedron: Asymmetry*, **8**, 2687–2691.
Dunning, T. H. Jr & Hay, P. J. (1977). *Methods of Electronic Structure Theory*, edited by H. F. Shaefer III, ch. 1, pp. 1–27. New York: Plenum Press.
Fasth, K. J., Hörnfeldt, K. & Långström, B. (1995). *Acta Chem. Scand.* **49**, 301–304.
Fasth, K. J. & Långström, B. (1990). *Acta Chem. Scand.* **44**, 720–725.
Gee, A. D. & Långström, B. (1991). *J. Chem. Soc. Perkin Trans. 1*, p. 215.
Granovsky, A. A. (2003). *PC GAMESS* version 6.3, build number 2260. http://classic.chem.msu.su/gran/gamess/index.html.
Jirman, J., Nádvorník, M. Sopková, J. & Popkov, A. (1998). *Magn. Reson. Chem.* **36**, 351–355.
Jirman, J. & Popkov, A. (1995). *Collect. Czech. Chem. Commun.* **60**, 990–998.
Koritsanszky, T., Howard, S. T., Su, Z., Mallinson, P. R., Richter, T. & Hansen, N. K. (1997). *XD, Computer Program Package for Multipole Refinement and Analysis of Electron Densities from Diffraction Data.* Free University of Berlin, Germany.
Kožíšek, J., Hansen, N. K. & Fuess, H. (2002). *Acta Cryst.* B**58**, 463–470.
Långström, B., Kihlberg, T., Bergström, M., Antoni, G., Björkman, M., Forngren, B. H., Forngren, T., Hartvig, P., Markides, K., Yngve, U. & Ogren, M. (1999). *Acta Chem. Scand.* **53**, 651–669.
Nádvorník, M. & Popkov, A. (2002). *Green Chem.* **4**, 71–72.
Paulmann, C. (2001). *SAPRO, Program for Scaling the SAINT Frames.* Personal communication.
Plenevaux, A., Al-Darwich, M. J., Lemaire, C., Delfiore, G. & Comar, D. (1994) *Appl. Radiat. Isot.* **45**, 361–369.
Popkov, A., Gee, A., Nádvorník, M. & Lyčka, A. (2002). *Transition Met. Chem.* **27**, 884–887.
Popkov, A., Langer, V., Manorik, P. A. & Weidlich, T. (2003). *Transition Met. Chem.*, **28**, 475–481.
Popkov, A., Nádvorník, M., Kružberská, P., Lyčka, A., Eisenhut, M. & Gillings, N. M. (2003). Proceedings of the 15th International Symposium on Radiopharmaceutical Chemistry, 10–15 August 2003, Sydney, Australia. *J. Labelled Comp. Radiopharm.* **46**, S227.
Rajagopal, S., Venkatachalam, T. K., Conway, T. & Diksic, M. (1992). *Appl. Radiat. Isot.* **43**, 979–987.
Rappe, A. K., Smedley, T. A. & Goddard, W. A. (1981). *J. Phys. Chem.* **85**, 2607–2611.
Schmidt, M. W., Balridge, K. K., Boatz, J. A., Elbert, S. T., Gordon, M. S., Jensen, J. J., Koseki, S., Matsunaga, N., Nguyen, K. A., Su, S., Windus, T. L., Dupuis, M. & Montgomery, J. A. (1993). *J. Comput. Chem.* **14**, 1347–1347.
Sheldrick, G. M. (2002). *SADABS*, Version 2.06, *Empirical Absorption Correction Program*. University of Göttingen, Germany.
Slouf, M., Holý, A., Petříček, V. & Císařová, I. (2002). *Acta Cryst.* B**58**, 519–529.
Vaalburg, W., Beerling-van der Molen, H. D., Reiffers, S., Rijskamp, A., Woldring, M. G. & Wynberg, H. (1976). *Int. J. Appl. Radiat. Isot.* **27**, 153–157.